

Accepted Manuscript

Lead removal by a reusable gel cation exchange resin containing nano-scale zero valent iron

Nopphorn Chanthapon, Sudipta Sarkar, Pinit Kidkhunthod, Surapol Padungthon

PII: S1385-8947(17)31482-1
DOI: <http://dx.doi.org/10.1016/j.cej.2017.08.133>
Reference: CEJ 17585

To appear in: *Chemical Engineering Journal*

Received Date: 29 May 2017
Revised Date: 29 August 2017
Accepted Date: 31 August 2017

Please cite this article as: N. Chanthapon, S. Sarkar, P. Kidkhunthod, S. Padungthon, Lead removal by a reusable gel cation exchange resin containing nano-scale zero valent iron, *Chemical Engineering Journal* (2017), doi: <http://dx.doi.org/10.1016/j.cej.2017.08.133>

This is a PDF file of an unedited manuscript that has been accepted for publication. As a service to our customers we are providing this early version of the manuscript. The manuscript will undergo copyediting, typesetting, and review of the resulting proof before it is published in its final form. Please note that during the production process errors may be discovered which could affect the content, and all legal disclaimers that apply to the journal pertain.



Lead removal by a reusable gel cation exchange resin containing nano-scale zero valent iron

Nopphorn Chanthapon¹, Sudipta Sarkar², Pinit Kidkhunthod³, Surapol Padungthon^{1,4,*}

¹Department of Environmental Engineering, Faculty of Engineering, Khon Kaen University,
Khon Kaen, 40002, Thailand

²Department of Civil Engineering, Indian Institute of Technology Roorkee,
Uttarakhand, 247667, India

³Synchrotron Light Research Institute, 111 University Avenue, Muang District,
Nakhon Ratchasima, 30000, Thailand

⁴Advanced Functional Nanomaterials & Membrane for Environmental Remediation
(AFMFR) Laboratory, Khon Kaen University, Khon Kaen, 40002, Thailand

*Corresponding author. Tel.: +669 946 9530; Email address: surapolp@kku.ac.th

Department of Environmental Engineering, Khon Kaen University, 123 Moo 16, Mittraphap
Road, Khon Kaen, 40002, Thailand

Abstract

The practical applications of nano-scale zero valent iron (nZVI) particles in flow-through treatment systems are limited due to unfavorable mechanical and hydraulic properties caused by their tiny size. On the other hand, nZVI, when dispersed within suitable host material, can overcome these limitations to have synergistic improvement in its adsorption capacity. This study aims to synthesize, characterize, validate the performance of hybrid cation gel exchanger dispersed with nZVI particles, named as C100-Fe⁰, for selective trace Pb(II) removal from contaminated water. C100-Fe⁰ had Fe content of approximately 22% w/w as determined by double acid digestion method. The characterization studies revealed that nZVI particles of size range 20 nm were well dispersed throughout the gel phase of the polymeric resin beads; XANES spectral analysis confirmed the presence of zero oxidation state of Fe nanoparticles within both the newly synthesized and regenerated C100-Fe⁰. Equilibrium batch studies demonstrated that Pb(II) adsorption capacity was unaffected by the presence of high concentration of competing ions such as Na⁺ and Ca²⁺ ions whereas, presence of SiO₂ decreased the capacity. The batch adsorption isotherm fitted well with Freundlich model. During column study with C100-Fe⁰, breakthrough of USEPA permissible limit of 15 µg/L was observed after the passage of 4,200 bed volumes of challenge water (NSF/ANSI Std.53) having Pb(II) concentration of 150 µg/L. More than 87% of adsorbed Pb (II) could be recovered within 15 bed volumes during regeneration with acid. Wide availability and low price of iron salts as well as of cation exchange resins, combined with the possible reusability make C100-Fe⁰ an attractive option for use in the field for removal of Pb(II) from contaminated water.

Key words: Lead, Nanoscale Zero Valent Iron, Adsorption, XANES, EXAFS

1. Introduction

The problem of heavy metal contamination in the environment is a major concern due to their toxicity and tendency to accumulate and bio-magnify within the food chain, causing wider damage to the ecosystem. Most of these heavy metals can be extremely toxic even at trace concentrations. Lead (Pb^{2+}) is one such toxic heavy metal that is released to the environment in large quantities every year. The sources of lead released into the environment can be both natural weathering processes and anthropogenic activities namely, electroplating, battery manufacturing, mining. In human being, lead is known to be accumulated mainly in kidneys, muscles, bones, nervous, and blood circulatory system causing several manifestations such as abdominal pain, fatigue, depression/mood changes, diminished cognitive performance and hand dexterity[1-4]. The USEPA (EPA, 2013) has set a permissible limit of 15 $\mu\text{g/L}$ in drinking water while Thailand Pollution Control Department (PCD) has set the standard of lead in the drinking and industrial effluents as 50 and 200 $\mu\text{g/L}$, respectively.

In order to comply with the regulatory limits, various technologies relying on conventional methods such as chemical precipitation, ion-exchange, and reverse osmosis have been adopted [5-7]. However, each of these methods suffers from one or more of the following drawbacks: high cost, generation of voluminous sludge, and poor removal efficiency due to high solubility product values of precipitating salts. In contrast, removal using adsorption shows higher efficiency and better economics as a result of potential for selective removal, regeneration and reuse of the adsorbent, and recovery of metals from wastewater.

Nanoscale zero-valent iron (nZVI) particles have shown good potential for removal of various metals such as Co^{2+} , Cu^{2+} , Pb^{2+} , Ni^{2+} from contaminated water and wastewater [8]. However, bare nZVI particles also suffer from disadvantages such as formation of

aggregates, reduction in specific surface area, production of a less negative redox potential, high pressure drop in fixed-bed column operations, low-to no- reusability, lack of durability and mechanical strength. In order to solve this problem, several attempts have been made to immobilize the n-ZVI into porous host materials. For the last 5 years, nZVI supported various materials have been widely investigated. They can be classified as (1) natural minerals such as pillared clay [9], pumice granular [10, 11], acid activated sepiolites [12, 13], montmorillonite [14-16], kaolin [17], bentonite [18, 19], zeolite [20, 21], biochar [22, 23], and char coal [24]; (2) biomaterials namely, aquatic plant *Azolla filiculoides* [25], walnut shell [26], macroporous alginate [27, 28]; and (3) synthetic materials such as anion exchange resin [29], chelating resin [30], mesoporous silica carbon [26], activated carbon [31, 32], cationic resin [33], graphene oxide [34, 35], magnesium (hydr)oxide [36, 37], layered double hydroxide [38, 39], titanate nanotube [40], carbon nanotube [41], and porous carbon sheet [42]. However, most of the studies focused onto the basic equilibrium batch study only. They lacked the use of column experiments as well as in depth study about the phase change and adsorption mechanism to elucidate interaction between Pb^{2+} and nZVI.

From the previous studies, it was understood that toxic heavy metal cations can be concentrated inside a cation exchanger having negatively charged (SO_3^-) fixed functional groups due to the Donnan membrane effect [43]. Therefore, the dispersion of nZVI inside a cation exchanger host should have improved potential to remove the target heavy metals. Note that, the cation exchangers alone can be used for the removal of heavy metal ions such as Pb^{2+} , Cu^{2+} , Ni^{2+} , etc. However, most of contaminated water has, apart from these heavy metal ions, other competing cations such as Ca^{2+} , Na^+ , etc. at a much higher concentrations compared to these heavy metal ions. Therefore, unless there is presence of any specific interaction other than electrostatic interactions for these trace heavy metal ions, it is not possible to effectively remove the target heavy metal cations from the background of the

other commonly occurring cations. Chelating resins with specific functional groups such as iminodiacetic acid exhibit high selectivity toward heavy metals compared to these competing cations. However, they have limited applications, primarily due to the high cost of these chelating resins.

This research was taken up to develop a reusable gel cation exchange resin containing nano-scale zerovalent iron (C100-Fe⁰) for trace lead removal from the natural water sources. To the best of our knowledge, this is the first instance to show that impregnating nZVI into a gel type cation exchange resin as a host material improves the target Pb²⁺ removal capacity from contaminated water. The mechanism behind the superior Pb²⁺ removal by a hybrid cation exchanger impregnated with nanoscale zero valent iron (C100-Fe⁰) is illustrated in the **Fig. 1**. In the presence of dissolved oxygen or other oxidants, nZVI gets oxidized to Fe²⁺/Fe³⁺ and subsequently, there is a formation of Fe²⁺/Fe³⁺ oxide layer as shell on the top of the core, which is still Fe⁰ or zero valent iron. Because of high density of negatively charge fixed functional groups (SO₃⁻), Pb²⁺ ions are attracted inside the hybrid material due to the Donnan membrane effect and then get adsorbed onto the surface of iron oxide on the dispersed nZVI, through the formation of inner sphere complex. The objectives of this study were to: (1) synthesize a reusable gel cation exchange resin containing nano-scale zero valent iron (C100-Fe⁰), (2) perform characterization of the C100-Fe⁰ through XRD, SEM-EDX, TEM, XANES, EXAFS and pH_{pzc} analyses, (3) investigate the effects of pH and competing ions, on the adsorption, equilibrium, and kinetics, and (4) assess the lead removal efficiency and reusability through fixed-bed column runs.

Space for Fig.1

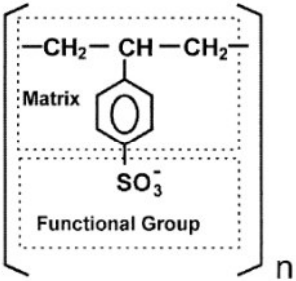
Fig. 1 Diagram of a reusable gel cation exchanger containing nano-scale zero valent iron (C100-Fe⁰).

2. Materials and methods

2.1 Materials and chemicals

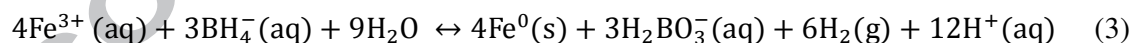
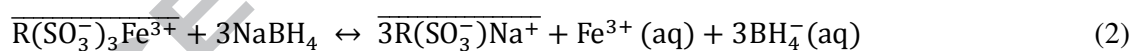
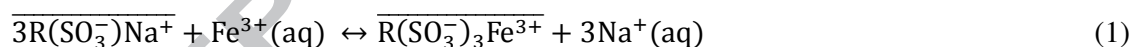
Analytical grade chemical reagents namely, lead nitrate ($\text{Pb}(\text{NO}_3)_2$), iron (III) chloride hexahydrate ($\text{FeCl}_3 \cdot 6\text{H}_2\text{O}$), sodium borohydride (NaBH_4), absolute ethanol ($\text{C}_2\text{H}_6\text{O}$), sodium hydroxide (NaOH), and hydrochloric acid (HCl) were used in this study. The pH was adjusted by using 0.1 M sodium hydroxide (NaOH) or 0.1 M nitric acid (HNO_3), depending on the requirement. The cation exchange resins (C100 and C145) and granular activated carbon (FILTRASORB 600) used in this study were kindly provided by M/S Purolite and Calgon Carbon Company, respectively. **Table 1** provides salient properties of the cation exchanger used in the study; however, no particular endorsement is implied; similar cation exchange resin and GAC from other manufacturers can also be used.

Table 1. Salient properties of polymeric cation exchangers

Properties	Purolite C100	Purolite C145
Structure	Polystyrene crosslinked with divinylbenzene	
		
Functional group	Gel Sulfonic acid	Macroporous Sulfonic acid
Reversible swelling, $\text{Na}^+ > \text{H}^+$	8%	6%
Exchange capacity	2 (eq/L) Na^+ form	1.5 (eq/L) Na^+ form
Moisture retention Na^+ form	44-48%	55-60%

2.2 Preparation of hybrid nano-adsorbents

For the synthesis of different hybrid materials, cation exchangers (C100 and C145) and granular activated carbon (GAC) were used as support material in which nano-scale zero valent iron particles (nZVI) were immobilized in situ via two steps as shown in eq. 1-3. First, Fe^{3+} ions were incorporated within the porous support via adsorption and/ or ion exchange at the respective functional groups of the porous support. Next, the adsorbed Fe^{3+} ions were reduced to Fe^0 by subjecting the porous support material to NaBH_4 solution. Briefly, 10 g of cation exchange resin or GAC was added to 80 mL of 5% w/v of $\text{FeCl}_3 \cdot 6\text{H}_2\text{O}$ solution kept in a 250 mL polyethylene bottle. The mixtures were shaken in a gyratory shaker for 3 hours at room temperature 24 ± 1.0 °C, and then the resultant solution was filtered to separate the solid beads or GAC before they were air dried for 12 hrs. The dried resin or GAC was then transferred into 80 mL of 0.5% NaBH_4 solution kept in a beaker and the mixture was shaken for 1 hr. The cation exchange resin or GAC which was now expected to get impregnated with nZVI dispersed within, was drained, washed with deoxygenated DI water, and was stored in ethanol solution so as to prevent it from any further oxidation .



2.3 Characterization studies

Characterizations of C100- Fe^0 were performed by X-ray diffraction (XRD, Bruker D8 Advance), scanning electron microscope with energy dispersive X-ray (SEM-EDX, Hitachi S3000N), transmission electron microscope (TEM, JEOL JEM-2010F), and pH point of zero charge (pH_{pzc}). For XANES and EXAFS experiments, the Fe *K*-edge spectra were measured

in the fluorescence mode with a 4-channel Si drift detector at the SUT-NANOTEC-SLRI XAS beamline (BL5.2), Synchrotron Light Research Institute (Public Organization), Thailand. For the acquisition of all spectra, a Ge (220) double crystal monochromator with an energy resolution ($\Delta E/E$) of 2×10^{-4} was used to scan the synchrotron X-ray beam.

2.4 Batch equilibrium experiments

The batch experiments were conducted in order to investigate the effect of support materials (cation exchange resin (C100 and C145) and granular activated carbon (GAC)), loading cycles (1 to 4 cycles), solution pH (pH 4 to 7), and competing background ions (Ca^{2+} , Na^+ , SiO_2). The effect of support materials on the removal capacity was studied to find the most suitable supporting material for achieving highest lead removal efficiency. In this experiment, 0.2 g of each parent and hybrid materials were added into 0.5 L of solution containing Pb^{2+} ions at concentration of 15.0 mg/L and having pH of 5.0 ± 0.5 along with the presence of 100 mg/L each of Ca^{2+} and Na^+ used as background concentrations of co-occurring ions. After shaking for 38 hrs, the Pb^{2+} uptake capacities (q) of different hybrid materials were calculated based on mass balance and were represented as mg Pb^{2+} /g of hybrid adsorbent. Eq. 4 shows the mass balance based approach to calculate the equilibrium adsorption capacity.

$$q = \frac{V(C_0 - C_e)}{m} \quad (4)$$

where q is lead uptake capacity (mg Pb^{2+} /g adsorbent), V is the volume of test solution, C_0 and C_e are the initial and equilibrium concentrations of Pb^{2+} in the aqueous solution, respectively and m is the mass of the adsorbent used. The hybrid adsorbent that demonstrated highest Pb^{2+} uptake capacity was used for further batch and fixed-bed column investigations concerning effect of number of Fe loading cycles, characterization studies,

effect of solution pH, competing ions, and adsorption and desorption equilibrium and kinetics.

The effect of Fe loading cycles on the Pb^{2+} uptake capacity was investigated to optimize the preparation process of the hybrid adsorbent. For this study, the hybrid adsorbents prepared by varying the number of Fe loading cycles were chosen and their equilibrium Pb^{2+} adsorption capacity was determined by subjecting the same mass of adsorbent to solution containing 10 mg/L Pb^{2+} at pH 5.0 ± 0.5 with 100 mg/L each of Ca^{2+} and Na^+ ions. In order to determine the effect of solution pH on the adsorption capacity, the same amount of adsorbents was exposed to different identical solutions of same Pb^{2+} concentration but with pH varying from 4 to 7. The pH of the solutions was adjusted periodically during the course of batch experiment until stable using 0.1 M sodium hydroxide (NaOH) and/ or 0.1 M nitric acid (HNO_3). Effect of competing ions on the adsorption capacity was determined by subjecting the same mass of adsorbent to solutions containing Pb^{2+} concentration of 10 mg/L but with varying concentrations (50-200 mg/L) of the background competing entities such as Ca^{2+} , Na^+ and SiO_2 while the pH was maintained at 5.0 ± 0.5 .

In order to obtain adsorption equilibrium data for hybrid ion exchanger for adsorption of Pb^{2+} , 1.0 g of C100- Fe^0 was added into each of the 8 bottles containing solutions at Pb^{2+} concentrations of 5, 20, 40, 80, 100, 150, 200, and 400 mg /L at pH 5.0 ± 0.5 and the contents were shaken in a gyratory shaker at a speed of 100 rpm for 72 hours until equilibrium is attained. All samples were analyzed in duplicate with control. The equilibrium adsorption capacity was measured using eq. 4. Adsorption capacities of C100- Fe^0 at different equilibrium concentrations can be described by Langmuir and Freundlich sorption models indicated in equations 5 and 6, respectively;

$$q = \frac{QbC_e}{(1+bC_e)} \quad (5)$$

$$q = K_f C_e^{\frac{1}{n}} \quad (6)$$

where Q is the maximum lead uptake capacity (mgPb²⁺/g), b is the Langmuir adsorption constant (L/mg), K_f is the Freundlich constant indicated the relative adsorption capacity of the adsorbent (mg/g), and $1/n$ is the adsorption intensity. Pb²⁺ concentrations in the solutions were measured using Flame Atomic Absorption Spectrophotometer (FAAS) (Perkin Elmers, model AAnalyst 800). Before measurement, 10 mL of aqueous sample was acidified with 1.0 mL of 1.0 N HNO₃. For the kinetic study, 0.2 g of C100-Fe⁰ was added to 0.5 L of solution containing 10 mg /L Pb²⁺ at pH 5.0±0.5 in 1.0 L beaker. The contents were continuously stirred using a jar test apparatus. Aqueous samples were collected at predetermined time intervals up to 400 minutes after the start of the experiment. The Pb²⁺ adsorption rate by C100-Fe⁰ over time was calculated and fitted with the intraparticle diffusion model (Eq. 9) to explain the diffusion behavior.

2.5 Fixed-bed Column Runs and Regeneration

Fixed-bed column runs for all experiments were performed using an epoxy coated glass column with 11 mm diameter (Kimble Chase), a constant flow pump (Watson Marlow 505U) and a fraction collector (Eldex U200). Synthetic contaminated solution representing the natural water containing 150 µg/L of Pb²⁺ at pH 6.5 was prepared by following NSF/ANSI Std. 53 and used as feed water in fixed-bed column experiments. The effluent samples were collected by a fraction collector, and then Pb²⁺ contents were measured using a Graphite Furnace Atomic Adsorption Spectrophotometer (GFAAS) (Perkin Elmers, model AAnalyst 800). The regeneration was performed by the passage of a solution containing 2%

HNO₃ and 1% FeCl₃.6H₂O, followed by another solution having 0.5% NaBH₄ was used to regenerate the exhausted materials. **Fig. 2** shows a schematic diagram of the experimental setup containing fixed-bed column used for adsorption and regeneration runs. Typically, results of the column studies have been represented as a plot of normalized concentration i.e. fraction of concentration in the outlet, (C/C_0) vs. bed volumes (BVs). Note that BV represents the volume of water passed through the column per volume of the bed (C100-Fe).

Space for Fig.2

Fig. 2 Schematic diagram of the test setup for fixed-bed column runs and regeneration.

3. Results and Discussion

3.1 Selection of porous host for hybrid adsorbent: effect on the Pb²⁺ adsorption capacity

Fig. 3 shows the comparison between the Pb²⁺ adsorption capacities of different types of porous host materials and the hybrid adsorbents prepared by dispersing nZVI inside the host material. The same mass of each of the adsorbents were exposed to contaminated solutions of identical volume and composition. **Fig. 3** indicates that for all the host material, the hybrid material always showed better adsorption capacity than its virgin version. The highest Pb²⁺ uptake capacity was observed for the hybrid adsorbent C100-Fe⁰ which showed a capacity of approximately 22.5 mg Pb²⁺/g adsorbent whereas C145-Fe⁰ showed the second highest uptake capacity of approximately 18 mgPb²⁺/g adsorbent. Both the granular activated carbon (GAC) and its hybrid version showed much lower adsorption capacity. The results showed that dispersing nZVI in the porous host material helped improve Pb²⁺ uptake capacity. A closer look in **Table 1** reveals that the ion exchange capacity of the parent cation exchanger C100 is higher than that of C145. This means that, compared to C145, C100 shall

have much higher Donnan inclusion effect for cations, resulting in higher concentrations of partitioning of Pb^{2+} inside the cation exchanger. Therefore, given the same loading of nZVI inside the hybrid cation exchanger and other parameters being the same, C100 should result in higher equilibrium uptake of Pb^{2+} as compared to C145. The results also proved the above logical disposition. C100- Fe^0 demonstrated maximum uptake rate; it was considered for further experiments.

Functional group of the parent material can play an important role to enhance target pollutant removal capacity. In our earlier work, we found that arsenic and fluoride removal were greatly enhanced when hydrated Zr(IV) oxide nanoparticles were dispersed into the polymeric anion exchanger containing high density of fixed positively charge quaternary amine (R_4N^+) functional groups [44-46]. Based on the Donnan membrane principle, the hybrid nanoadsorbent could be engineered by using the suitable supported materials to achieve the synergistic adsorption effects [47]. The result from **Fig.3** confirmed that the Pb^{2+} uptake capacity from cation exchange based adsorbent was significantly greater than non-functional group GAC assuming the nZVI content in both material was not significant different.

Space for Fig.3

Fig.3 Batch equilibrium tests for lead removal using various adsorbents.

3.2 Effect of multiple loading cycles

Fig. 4 shows the effect of multiple Fe^0 loading cycles on the Fe^0 content on the C100- Fe^0 and also on the Pb^{2+} adsorption capacity of the hybrid adsorbent. As can be expected, the Fe^0 content of the hybrid adsorbent increased with the increase in the number of Fe loading cycle from 1 to 4. However, the incremental benefit of higher number of loading cycles

became smaller as the number of loading cycles increased. After 4 cycles of loading, the Fe^0 content reached to 225 mg Fe^0/g adsorbent. Pb^{2+} uptake capacity also followed the same trend as the Fe^0 loading; it reached to almost a constant value of 13 mg Pb^{2+}/g adsorbent. It may be noted that the sorption capacity did not increase in proportion to the increase in Fe^0 loading on the hybrid ion exchanger. The overall adsorption capacity did not increase in proportion to the increase in the Fe^0 -loading on the hybrid ion exchanger. The overall adsorption capacity depends on the surface area available for adsorption. Obviously, more Fe^0 loading should mean more nZVI inside the ion exchanger. However, higher Fe^0 loading does not necessarily mean that there was an increase of available surfaces for adsorption. There might be aggregation of nZVI nanoparticles inside the hybrid ion exchanger, resulting in lower adsorption capacity than expected.

Space for Fig.4

Fig. 4 Effect of nZVI loading cycles on the amount of iron dispersed within the hybrid cation exchanger and on the corresponding Pb^{2+} uptake capacity.

3.3 Characterization of the hybrid adsorbent C100- Fe^0

C100- Fe^0 was characterized through studies conducted using different imaging techniques. **Fig. 5** shows the results of scanning electron microscopy (SEM) and energy dispersive X-ray spectroscopy (EDX) study done on C100- Fe^0 . The SEM image in **Fig. 5A** shows that C100- Fe^0 were spherical bead-like in shape, having size range of approximately 500 μm . **Fig. 5B** shows the morphology of the gel type C100- Fe^0 in 10,000X magnification as obtained from the SEM study. An estimate of Fe content as obtained by EDX study of

C100-Fe⁰ is shown in **Fig. 5C**. The study revealed that the Fe content was approximately 10% by weight.

Space for Fig.5

Fig. 5 (A) Enlarged view photograph of the C100-Fe⁰ (~500 μm diameter bead); (B) SEM of gel-type C100-Fe⁰ (10,000X); (C) Energy dispersive X-ray spectroscopy (EDX) spectrum of the material (10% Fe w/w) including iron mapping.

Fig. 6 shows a transmission electron microscopy (TEM) micrograph of the interior of C100-Fe⁰. The size distribution Fe⁰ was studied using the Image J program and is also included in Fig 6. It shows that 97% particles were below 100 nm in size and about 50% of the particles had size of 20 nm or less. **Fig. 7** shows the XRD diffractograms of C100-Fe⁰. The XRD results of fresh and used C100-Fe⁰, when compared with that of the standard crystalline Fe₂O₃, did not show any appearance of definite peak in XRD analysis. It implied that C100-Fe⁰ had amorphous phase. The amorphous structure exhibits higher surface area as compared to the crystalline structure, which might result in high adsorption capacity.

Space for Fig.6

Fig. 6 Transmission electron microscopy (TEM) of C100-Fe⁰.

Space for Fig.7

Fig. 7 Comparison of XRD diffractograms between a freshly prepared C100-Fe⁰ and used C100-Fe⁰ with standard Fe₂O₃.

In order to reveal the valence states and local structure of Fe atoms in samples, XANES and EXAFS data were carefully analyzed. The normalized XANES and EXAFS data were processed after background subtraction in the pre-edge and post-edge regions using the Athena software which is included in an IFEFFIT package [48, 49]. **Fig. 8** shows the XANES

spectra for C100-Fe⁰ samples and the same was compared with that of Fe⁰, Fe²⁺ and Fe³⁺ standard samples. From XANES results, it can be concluded that the new synthesized material (C100-Fe⁰) had a mixed Fe oxidation state of zero (Fe⁰) and 2 (Fe²⁺). The XANES spectra of used C100-Fe⁰ resembled more with Fe³⁺ standard, suggesting that in the used adsorbent there was a structural change to the solid particles causing transformation of Fe⁰ and Fe²⁺ to the trivalent state of Fe (Fe³⁺). The XANES spectra of the regenerated C100-Fe⁰ matched with the freshly prepared C100-Fe⁰ suggesting that after regeneration, Fe³⁺ at the surface again transformed back to its original state.

Space for Fig.8

Fig. 8 XANES spectra for C100-Fe⁰ samples comparing with Fe⁰, Fe²⁺ and Fe³⁺ standards.

Additionally, in order to confirm an existence of Pb substitutions in C100-Fe⁰ structure, EXAFS results at Fe K-edge were carefully analyzed as presented in **Fig. 9A**. Similar works were reported using EXAFS and DFT techniques to elucidate the sorption mechanism between U(VI), Cu(II), and Sr(III) on graphene oxides (GO) through the formation of inner or outer sphere complexes [50-52]. In this study, EXAFS was used to confirm the presence of Pb(II) bonded with the surface of Fe(III) (hydr)oxide shell. The inter-atomic distances between Fe-Fe, Fe-O, and Fe-Pb were approximately found out (no phase shift correction) at 1.50 Å (peak A), 2.70 Å (peak B) and 3.30 Å (peak C), respectively. Especially, there is a broad peak at point C; the observed Fe-Pb bond distances are similar to the reports [53, 54] found in open literature on Fe-As bond distances which are in a range of 3.12 Å for edge sharing and 3.65 Å for corner or isolated bidentate sharing complexes. Thus, it might be concluded that Pb²⁺ adsorption on C100-Fe⁰ was a strong adsorption leading to formation of inner-sphere type complexes rather than outer-sphere type weak complexes where the mean distance of Pb atom from oxygen only surface was reported to be

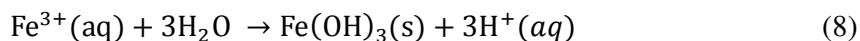
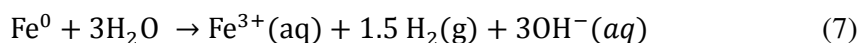
approximately 4.2 Å [55]. **Fig. 9B** illustrates a schematic of the proposed Pb²⁺ adsorption mechanism onto the surface of iron oxide through the formation of bidentate inner-sphere complex.

Space for Fig.9

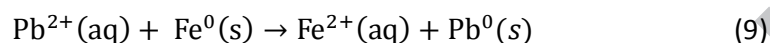
Fig. 9 (A) EXAFS results at Fe K-edge and (B) Proposed mechanism of Pb²⁺ adsorption onto the surface of iron oxide through the formation of bidentate inner-sphere complex.

3.4 Batch studies

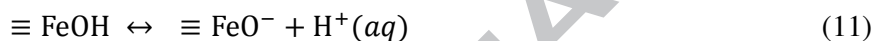
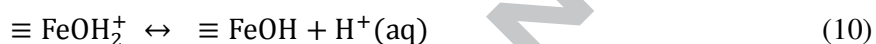
Fig. 10A shows a plot of the change in pH value (ΔpH) versus initial pH recorded before and long after a known mass of adsorbents was added to solutions having different pH values. The point of inflection or the initial pH value at which there is no change in the final pH value of the solution after the addition of the adsorbent is known as the point of zero charge (pH_{PZC}) of the adsorbent, a pH at which the net charge on any surface becomes equal to zero. It may be observed that the parent C100 and hybrid adsorbent C100-Fe⁰ exhibited pH_{PZC} values equal to 6.6 and 2.8, respectively. The inference is that the surface of C100-Fe⁰ becomes the negatively charged at pH > 2.8, rendering the adsorbent with capability of attracting positively charged moieties over a broad range of pH. At elevated pH, the dissolution kinetics of oxygen in water is high, so conversion of Fe⁰ into Fe³⁺ shall also be favored. During service cycle, the nZVI dispersed inside the C100-Fe0 was oxidized primarily by H₂O forming “core shell structure” as shown in the eq. 7-8.



Note that nZVI has a standard reduction potential of -0.440 V and is able to release electron quickly due to its large surface area. Since Pb(II) has standard reduction potential (-0.126) slightly higher than metallic iron, reduction of Pb(II) to Pb⁰ as shown in eq. 9 is slightly occurred.



Most of Pb²⁺ removal mechanisms come from adsorption onto the iron oxide occurred on the shell of nZVI particles. Based on the point of zero charge (PZC) of C100-Fe⁰, amorphous hydrated Fe(III) oxide (HFO) nanoparticles can be approximated as a diprotic acid with the following two acid dissociation constants (pKa) as shown in eq. 10-11:



At the pH greater than 2.8 (pH_{PZC}), the charge at the surface of HFO on the shell of core nZVI will deprotonated to $\equiv \text{FeO}^-$. Lead ions can be strongly adsorbed onto the surface of HFO nanoparticles via both Coulombic and LAB interactions. Under acidic conditions maintained during regeneration, the surface of ferric oxide formed on the shell structure of nZVI becomes protonated to FeOH_2^+ thereby forcing Pb²⁺ out of the surface through electrostatic repulsion, causing Pb²⁺ to desorb from the hybrid adsorbent. Hence, the solution pH is likely to be an important process parameter which should control the Pb²⁺ adsorption capacity of the adsorbent. We varied the solution pH from 4 to 7 so as to assess the Pb²⁺ uptake at different pH. **Fig.10B** shows the results of the study. Pb²⁺ uptake capacity increased with the increase in pH, and reached the highest value of approximately 14.5 mgPb²⁺/g adsorbent at pH 7. The pH was not increased beyond this point as practically it becomes expensive to raise the pH by adding alkali from outside.

Space for Fig.10

Fig. 10 (A) Δ pH versus initial pH of C100-Fe⁰ in 0.1 M NaCl solution at 298 K. (B) Effect of pH of C100-Fe⁰.

The real life use of the adsorbent shall demand a high degree of selectivity for the adsorption of Pb²⁺ because of the possible presence of other naturally occurring competing species in surface water, groundwater, or industrial wastewater. Three competing species (Na⁺, Ca²⁺, and SiO₂) were chosen to investigate such effect under varying concentration up to 200 mg/L. The result of the study is shown in **Fig.11**. It may be observed that the presence of Na⁺ and Ca²⁺ did not affect Pb²⁺ uptake capacity of C100-Fe⁰ whereas SiO₂ affected the adsorption capacity. Pb²⁺ ions, being d-block element, can make stable inner sphere complexes with hydrated ferric oxide surface via Lewis acid-base (LAB) interaction while Na⁺ and Ca²⁺ having outer electronic configuration like inert gases, cannot make inner sphere complexes with the ferric oxide surfaces. So, due to higher LAB interaction, the adsorption of Pb²⁺ is favored over Na⁺ and Ca²⁺ ions. Therefore, the presence of competing species such as Na⁺ and Ca²⁺ at higher concentrations could not interfere with the uptake of trace Pb²⁺ ions. Dissolved silica at high concentration is known to react with hydrated ferric oxide surface in the pH range between 5 and 6, to form surface groups such as FeSiO₃(OH)₄ and FeSi₂O₂(OH)₅ [56], which either interfere with the LAB or the electrostatic interactions between the hydrated ferric oxide and Pb²⁺ ions. At higher silica concentrations the sorption density on the ferric oxide surface is much higher, resulting in stronger interference.

Space for Fig.11

Fig. 11 Effect of competing ions on Pb(II) removal capacity.

The adsorption isotherms of C100-Fe were fitted with Langmuir as well as Freundlich models and all parameters were estimated and summarized in **Fig. 12**. The Freundlich

adsorption isotherm model showed a much better fit with the experimental results obtained.

This indicates that the adsorption is not a monolayer sorption as postulated in Langmuir's model; rather, it is a result of multilayer adsorption. Comparison of Pb^{2+} adsorption capacity on different hybrid nZVI materials in the literature is provided in **Table 2**. Although high capacity hybrid nanoadsorbent can be synthesized, powder form adsorbents were hardly applied using fixed-bed columns.

Space for Fig.12

Fig. 12 The comparison of Pb(II) adsorption by C100-Fe⁰ between Langmuir and Freundlich Models (Non Linear). **Fig. 13A** shows the change in the aqueous phase concentration of Pb^{2+} over time and **Fig. 13B** showed the normalized fractional uptake (F) of Pb^{2+} by C100-Fe⁰ versus time. Note that Pb^{2+} adsorption onto C100-Fe⁰ reached equilibrium at time of about 5 hrs after the beginning of the experiment. The detail of the intraparticle diffusion model was described extensively in eq. 12 [57].

$$F = \frac{q_t}{q_\infty} = 1 - \sum_{n=1}^{\infty} \frac{6\omega(\omega+1) \exp\left(\frac{D_{eff}\beta_n^2 t}{R^2}\right)}{9+9\omega+\beta_n^2\omega^2} \quad (12)$$

The solid lines in **Fig. 13A** and **13B** represent the model predictions of the intraparticle diffusion control kinetics. The best-fit effective intraparticle diffusivity, D_{ff} was computed to be equal to $12 \times 10^{-5} \text{ cm}^2/\text{s}$. This diffusivity parameter (D_{ff}) obtained from C100-Fe⁰ hybrid nanoadsorbent is higher than other hybrid polymeric supporting nanoparticles materials namely, $5 \times 10^{-11} \text{ cm}^2/\text{s}$ [58], $8 \times 10^{-11} \text{ cm}^2/\text{s}$ [59], $9 \times 10^{-11} \text{ cm}^2/\text{s}$ [44].

Space for Fig.13

Fig. 13 (A) Aqueous lead concentration versus time during the batch kinetic test using C100-Fe⁰, (B) fractional lead uptake (q_t/q_∞) versus time (t) from the batch kinetic test result in (A).

3.5 Fixed-bed column runs

In order to examine the performance of C100-Fe⁰ in comparison to the other adsorbents, series of column runs were performed with the challenge solution containing 150 µg/L of Pb²⁺ along with the background of competing ions through fixed bed columns containing different types of adsorbents under otherwise similar conditions. The time history plot of the outlet Pb²⁺ concentrations measured during the column runs are shown in **Fig. 14A**. The adsorbents used were C100, GAC, C100-Fe⁰ and GAC-Fe⁰. The column containing C100-Fe⁰ ran for the longest; it could treat contaminated water containing 150 µg/L Pb²⁺ to produce treated water having concentration below the USEPA drinking water standard (< 15 µg/L) at around 4,200 BVs whereas the parent cationic material (C100) could treat Pb²⁺ only until 1,800 BVs. For other two materials (GAC and GAC-Fe⁰), GAC-Fe⁰ could treat the contaminated water until 600 BVs whereas the GAC broke through at around 500 BVs.

Fig. 14 B, in the inset of **Fig. 14**, shows the profile of Pb²⁺ concentration in the effluent of the column with respect to BVs of regenerant when the exhausted column was regenerated following the protocol indicated in the material and methods section. During regeneration, almost 89 % of adsorbed Pb²⁺ ions could be recovered within approximately 15 BVs. After regeneration, C100-Fe⁰ was put in operation again under the identical condition as before. There is a chance that at low pH the iron oxide shell may partially get dissolved through formation of Fe³⁺ ion. However, even if such dissolution might have occurred, the liberated Fe³⁺ ion would have been strongly held back within by the cation exchanger through heterovalent ion exchange. To keep the dissolution of iron oxide coated onto the nZVI to as low as possible, diluted HNO₃ was used for regeneration. The regenerant also contained fresh FeCl₃ solution, which was followed up by NaBH₄ solution to deposit more nZVI. The regenerated adsorbent could still treat Pb²⁺ for approximately 3,800 BVs in the second run which was slightly less than the previous one. This suggests that the adsorbent can be reused

for number of cycles without any significant drop in the Pb^{2+} removal capacity. The spent regeneration solution containing high concentration of Pb^{2+} and Fe^{3+} can be disposed of safely by co-precipitation method.

Space for Fig.14

Fig. 14 (A) Pb(II) removal on fixed-bed column runs using four different materials, namely, hybrid cation (C100-Fe^0), hybrid granular activated carbon support nZVI (GAC-Fe^0), commercial cation exchange resin (C100), and commercial granular activated carbon (GAC) (B) Regeneration of C100-Fe^0 .

4. Conclusion

The experimental results showed that hybrid C-100 cation exchange resins dispersed with nano-scale iron particles in its pores could demonstrate high capacity for selective removal of Pb^{2+} ions from a synthetic wastewater containing naturally occurring competing cations. The hybrid resin, C100-Fe^0 was prepared in the laboratory from inexpensive raw materials through simple synthesis process. The highest Pb^{2+} uptake capacity found at pH 7.0. Out of the known competing species, only SiO_2 was observed to affect the Pb^{2+} removal capacity of C100-Fe^0 . The fixed-bed column runs confirmed that when subjected to a synthetic wastewater solution containing $150 \mu\text{g/L}$ of Pb^{2+} , the C100-Fe^0 column could treat 4,200 BV of wastewater before reaching a breakthrough concentration corresponding to USEPA drinking water standard at $15 \mu\text{g/L}$. The study also revealed that the hybrid adsorbent was regenerable and there was no significant loss in its capacity after regeneration.

Acknowledgements

We acknowledge the helpful discussion from Prof. Kriengsak Srisuk. The authors are grateful for financial support from the Thailand Research Fund (TRG5880160), Center for Thai Government Science and Technology Scholarship Students (CSTS), National Science and Technology Development Agency (NSTDA), The Synchrotron Research Funding from Khon Kaen University (2559-KKU-SLRI-01-03), and Synchrotron Light Research Institute for providing facilities of collection XANES and EXAFS data, and Research Center for Environmental and Hazardous Substance Management (EHSM), Khon Kaen University.

References

- [1] D.M. Mottier, E. Cargnel, Abdominal pain as a presentation by lead poisoning. Case report, *Arch. Argent. Pediatr.* 115 (2017) E96-E98.
- [2] C.M. Lee, A.R. Terrizzi, C. Bozzini, A.E. Pineiro, M.I. Conti, M.P. Martinez, Chronic lead poisoning magnifies bone detrimental effects in an ovariectomized rat model of postmenopausal osteoporosis, *Exp. Toxicol. Pathol.* 68 (2016) 47-53.
- [3] V.A. Miracle, Lead poisoning in children and adults, *Dimens. Crit. Care Nurs.* 36 (2017) 71-73.
- [4] S. Kianoush, M. Balali-Mood, S.R. Mousavi, V. Moradi, M. Sadeghi, B. Dadpour, O. Rajabi, M.T. Shakeri, Comparison of therapeutic effects of garlic and d-penicillamine in patients with chronic occupational lead poisoning, *Basic Clin. Pharmacol. Toxicol.* 110 (2012) 476-481.
- [5] I. Kabdasli, O. Tunay, P. Teymur, Lead treatment alternatives by chemical precipitation, *Fresenius Environ. Bull.* 26 (2017) 527-532.
- [6] M.M. Matlock, B.S. Howerton, D.A. Atwood, Chemical precipitation of lead from lead battery recycling plant wastewater, *Indus. Eng. Chem. Res.* 41 (2002) 1579-1582.
- [7] A. Bozecka, M. Orlof-Naturalna, S. Sanak-Rydlowska, Removal of lead, cadmium and copper ions from aqueous solutions by using ion exchange resin C 160, *Gospod. Surowcami Miner.* 32 (2016) 129-139.
- [8] Y. Zou, X. Wang, A. Khan, P. Wang, Y. Liu, A. Alsaedi, T. Hayat, X. Wang, Environmental Remediation and Application of Nanoscale Zero-Valent Iron and Its Composites for the Removal of Heavy Metal Ions: A Review, *Environ. Sci. Technol.* 50 (2016) 7290-7304.

- [9] Y.M. Li, W. Cheng, G.D. Sheng, J.F. Li, H.P. Dong, Y. Chen, L.Z. Zhu, Synergetic effect of a pillared bentonite support on SE(VI) removal by nanoscale zero valent iron, *Appl. Catal., B* 174 (2015) 329-335.
- [10] T.Y. Liu, Y.L. Yang, Z.L. Wang, Y.Q. Sun, Remediation of arsenic(III) from aqueous solutions using improved nanoscale zero-valent iron on pumice, *Chem. Eng. J.* 288 (2016) 739-744.
- [11] T.Y. Liu, Z.L. Wang, X.X. Yan, B. Zhang, Removal of mercury (II) and chromium (VI) from wastewater using a new and effective composite: Pumice-supported nanoscale zero-valent iron, *Chem. Eng. J.* 245 (2014) 34-40.
- [12] A.J. Habish, S. Lazarevic, I. Jankovic-Castvan, B. Jokic, J. Kovac, J. Rogan, D. Janackovic, R. Petrovic, Nanoscale zerovalent iron (nZVI) supported by natural and acid-activated sepiolites: the effect of the nZVI/support ratio on the composite properties and Cd²⁺ adsorption, *Environ. Sci. Pollut. Res.* 24 (2017) 628-643.
- [13] R.B. Fu, Y.P. Yang, Z. Xu, X. Zhang, X.P. Guo, D.S. Bi, The removal of chromium (VI) and lead (II) from groundwater using sepiolite-supported nanoscale zero-valent iron (S-NZVI), *Chemosphere* 138 (2015) 726-734.
- [14] J. Wang, G.J. Liu, C.C. Qi, C.C. Zhou, Synthesis and characterization of montmorillonite-supported zero-valent iron nanoparticles with application for preconcentration of zinc, *Anal. Lett.* 49 (2016) 2766-2782.
- [15] B.W. Hu, F. Ye, X.M. Ren, D.L. Zhao, G.D. Sheng, H. Li, J.Y. Ma, X.K. Wang, Y.Y. Huang, X-ray absorption fine structure study of enhanced sequestration of U(VI) and Se(IV) by montmorillonite decorated with zero-valent iron nanoparticles, *Environ. Sci. : Nano* 3 (2016) 1460-1472.
- [16] S. Bhowmick, S. Chakraborty, P. Mondal, W. Van Renterghem, S. Van den Berghe, G. Roman-Ross, D. Chatterjee, M. Iglesias, Montmorillonite-supported nanoscale zero-valent iron for removal of arsenic from aqueous solution: Kinetics and mechanism, *Chem. Eng. J.* 243 (2014) 14-23.
- [17] C. Wang, Z. Xu, G. Ding, X.X. Wang, M.J. Zhao, S.S.H. Ho, Y.C. Li, Comprehensive study on the removal of chromate from aqueous solution by synthesized kaolin supported nanoscale zero-valent iron, *Desalin. Water Treat.* 57 (2016) 5065-5078.
- [18] Z.H. Diao, X.R. Xu, D. Jiang, L.J. Kong, Y.X. Sun, Y.X. Hu, Q.W. Hao, H. Chen, Bentonite-supported nanoscale zero-valent iron/persulfate system for the simultaneous removal of Cr(VI) and phenol from aqueous solutions, *Chem. Eng. J.* 302 (2016) 213-222.
- [19] Z.H. Diao, X.R. Xu, H. Chen, D. Jiang, Y.X. Yang, L.J. Kong, Y.X. Sun, Y.X. Hu, Q.W. Hao, L. Liu, Simultaneous removal of Cr(VI) and phenol by persulfate activated with bentonite-supported nanoscale zero-valent iron: Reactivity and mechanism, *J. Hazard. Mater.* 316 (2016) 186-193.

- [20] X.K. Kong, Z.T. Han, W. Zhang, L. Song, H. Li, Synthesis of zeolite-supported microscale zero-valent iron for the removal of Cr⁶⁺ and Cd²⁺ from aqueous solution, *J. Environ. Manage.* 169 (2016) 84-90.
- [21] S.A. Kim, S. Kamala-Kannan, K.-J. Lee, Y.-J. Park, P.J. Shea, W.-H. Lee, H.-M. Kim, B.-T. Oh, Removal of Pb(II) from aqueous solution by a zeolite–nanoscale zero-valent iron composite, *Chem. Eng. J.* 217 (2013) 54-60.
- [22] H.J. Su, Z.Q. Fang, P.E. Tsang, L.C. Zheng, W. Cheng, J.Z. Fang, D.Y. Zhao, Remediation of hexavalent chromium contaminated soil by biochar-supported zero-valent iron nanoparticles, *J. Hazard. Mater.* 318 (2016) 533-540.
- [23] Z.G. Liu, F. Zhang, S.K. Hoekman, T.T. Liu, C. Gai, N.N. Peng, Homogeneously dispersed zerovalent iron nanoparticles supported on hydrochar-derived porous carbon: simple, in situ synthesis and use for dechlorination of PCBs, *ACS Sustainable Chem. Eng.* 4 (2016) 3261-3267.
- [24] D.Q. Liu, Z.R. Liu, C.F. Wang, Y. Lai, Removal of uranium(VI) from aqueous solution using nanoscale zero-valent iron supported on activated charcoal, *J. Radioanal. Nucl. Chem.* 310 (2016) 1131-1137.
- [25] M. Arshadi, M.K. Abdolmaleki, F. Mousavinia, S. Foroughifard, A. Karimzadeh, Nano modification of NZVI with an aquatic plant *Azolla filiculoides* to remove Pb(II) and Hg(II) from water: Aging time and mechanism study, *J. Colloid Interface Sci.* 486 (2017) 296-308.
- [26] F.C. Yang, Y.Y. He, S.Q. Sun, Y. Chang, F. Zha, Z.Q. Lei, Walnut shell supported nanoscale Fe⁰ for the removal of Cu(II) and Ni(II) ions from water, *J. Appl. Polym. Sci.* 133 (2016).
- [27] C.S. Lee, J. Gong, C.V. Huong, D.S. Oh, Y.S. Chang, Macroporous alginate substrate-bound growth of Fe⁰ nanoparticles with high redox activities for nitrate removal from aqueous solutions, *Chem. Eng. J.* 298 (2016) 206-213.
- [28] J.F. Huang, Y.T. Li, J.H. Wu, P.Y. Cao, Y.L. Liu, G.B. Jiang, Floatable, macroporous structured alginate sphere supporting iron nanoparticles used for emergent Cr(VI) spill treatment, *Carbohydr. Polym.* 146 (2016) 115-122.
- [29] F. Liu, C. Shan, X.L. Zhang, Y.Y. Zhang, W.M. Zhang, B.C. Pan, Enhanced removal of EDTA-chelated Cu(II) by polymeric anion-exchanger supported nanoscale zero-valent iron, *J. Hazard. Mater.* 321 (2017) 290-298.
- [30] J.L. Shi, S.N. Yi, C. Long, A.M. Li, Effect of Fe loading quantity on reduction reactivity of nano zero-valent iron supported on chelating resin, *Front. Environ. Sci. Eng.* 9 (2015) 840-849.
- [31] V. Gosu, B.R. Gurjar, R.Y. Surampalli, T.C. Zhang, Treatment of pyridine-bearing wastewater by nano zero-valent iron supported on activated carbon derived from agricultural waste, *Desalin. Water Treat.* 57 (2016) 6250-6260.

- [32] J. Busch, T. Meissner, A. Potthoff, S. Bleyl, A. Georgi, K. Mackenzie, R. Trabitzzsch, U. Werban, S.E. Oswald, A field investigation on transport of carbon-supported nanoscale zero-valent iron (nZVI) in groundwater, *J. Contam. Hydrol.* 181 (2015) 59-68.
- [33] A. Toli, K. Chalastara, C. Mystrioti, A. Xenidis, N. Papassiopi, Incorporation of zero valent iron nanoparticles in the matrix of cationic resin beads for the remediation of Cr(VI) contaminated waters, *Environ. Pollut.* 214 (2016) 419-429.
- [34] M.Y. Fan, T.J. Li, J.W. Hu, R.S. Cao, Q. Wu, X.H. Wei, L.Y. Li, X.D. Shi, W.Q. Ruan, Synthesis and characterization of reduced graphene oxide-supported nanoscale zero-valent iron (nZVI/rGO) composites used for Pb(II) removal, *Materials* 9 (2016).
- [35] S. Yang, C. Chen, Y. Chen, J. Li, D. Wang, X. Wang, W. Hu, Competitive Adsorption of PbII, NiII, and SrII Ions on Graphene Oxides: A Combined Experimental and Theoretical Study, *ChemPlusChem* 80 (2015) 480-484.
- [36] A. Siciliano, Removal of Cr(VI) from Water Using a New Reactive Material: Magnesium Oxide Supported Nanoscale Zero-Valent Iron, *Materials* 9 (2016).
- [37] M.H. Liu, Y.H. Wang, L.T. Chen, Y. Zhang, Z. Lin, Mg(OH)₂ supported nanoscale zero valent iron enhancing the removal of Pb(II) from aqueous solution, *ACS Appl. Mater. Interfaces* 7 (2015) 7961-7969.
- [38] G.D. Sheng, Y.N. Tang, W.S. Linghu, L.J. Wang, J.X. Li, H. Li, X.K. Wang, Y.Y. Huang, Enhanced immobilization of ReO₄⁻ by nanoscale zerovalent iron supported on layered double hydroxide via an advanced XAFS approach: Implications for TcO₄⁻ sequestration, *Appl. Catal. , B* 192 (2016) 268-276.
- [39] G. Sheng, J. Hu, H. Li, J. Li, Y. Huang, Enhanced sequestration of Cr(VI) by nanoscale zero-valent iron supported on layered double hydroxide by batch and XAFS study, *Chemosphere* 148 (2016) 227-232.
- [40] B. Hu, G. Chen, C. Jin, J. Hu, C. Huang, J. Sheng, G. Sheng, J. Ma, Y. Huang, Macroscopic and spectroscopic studies of the enhanced scavenging of Cr(VI) and Se(VI) from water by titanate nanotube anchored nanoscale zero-valent iron, *J. Hazard. Mater.* 336 (2017) 214-221.
- [41] G. Sheng, A. Alsaedi, W. Shammakh, S. Monaque, J. Sheng, X. Wang, H. Li, Y. Huang, Enhanced sequestration of selenite in water by nanoscale zero valent iron immobilization on carbon nanotubes by a combined batch, XPS and XAFS investigation, *Carbon* 99 (2016) 123-130.
- [42] X. Wang, S. Zhang, J. Li, J. Xu, X. Wang, Fabrication of Fe/Fe₃C@porous carbon sheets from biomass and their application for simultaneous reduction and adsorption of uranium(vi) from solution, *Inorg. Chem. Front.* 1 (2014) 641-648.
- [43] P. Puttamraju, A.K. SenGupta, Evidence of tunable on-off sorption behaviors of metal oxide nanoparticles:role of ion exchanger support, *Ind. Eng. Chem. Res.* 45 (2006) 7737-7742.

- [44] S. Padungthon, M. German, S. Wiriathamcharoen, A.K. SenGupta, Polymeric anion exchanger supported hydrated Zr(IV) oxide nanoparticles: A reusable hybrid sorbent for selective trace arsenic removal, *React. Funct. Polym.* 93 (2015) 84-94.
- [45] S. Padungthon, J.Z. Li, M. German, A.K. SenGupta, Hybrid anion exchanger with dispersed zirconium oxide nanoparticles: A durable and reusable fluoride-selective sorbent, *Environ. Eng. Sci.* 31 (2014) 360-372.
- [46] S. Padungthon, J.E. Greenleaf, A.K. Sengupta, Carbon dioxide sequestration through novel use of ion exchange fibers (IX-fibers), *Chem. Eng. Res. Des.* 89 (2011) 1891-1900.
- [47] S. Sarkar, A.K. Sengupta, P. Prakash, The Donnan membrane principle: opportunities for sustainable engineered processes and materials, *Environ. Sci. Technol.* 44 (2010) 1161-1166.
- [48] M. Newville, EXAFS analysis using FEFF and FEFFIT, *J. Synchrotron Radiat.* 8 (2001) 96-100.
- [49] B. Ravel, M. Newville, ATHENA, ARTEMIS, HEPHAESTUS: data analysis for X-ray absorption spectroscopy using IFEFFIT, *J. Synchrotron Radiat.* 12 (2005) 537-541.
- [50] Y. Sun, S. Yang, Y. Chen, C. Ding, W. Cheng, X. Wang, Adsorption and desorption of U(VI) on functionalized graphene oxides: A combined experimental and theoretical study, *Environ. Sci. Technol.* 49 (2015) 4255-4262.
- [51] Y. Sun, Z.-Y. Wu, X. Wang, C. Ding, W. Cheng, S.-H. Yu, X. Wang, Macroscopic and microscopic investigation of U(VI) and Eu(III) adsorption on carbonaceous nanofibers, *Environ. Sci. Technol.* 50 (2016) 4459-4467.
- [52] W. Cheng, C. Ding, Q. Wu, X. Wang, Y. Sun, W. Shi, T. Hayat, A. Alsaedi, Z. Chai, X. Wang, Mutual effect of U(vi) and Sr(ii) on graphene oxides: evidence from EXAFS and theoretical calculations, *Environ. Sci: Nano* 4 (2017) 1124-1131.
- [53] G.A. Waychunas, B.A. Rea, C.C. Fuller, J.A. Davis, Surface chemistry of ferrihydrite: Part 1. EXAFS studies of the geometry of coprecipitated and adsorbed arsenate, *Geochim. Cosmochim. Acta* 57 (1993) 2251-2269.
- [54] A.C.Q. Ladeira, V.S.T. Ciminelli, H.A. Duarte, M.C.M. Alves, A.Y. Ramos, Mechanism of anion retention from EXAFS and density functional calculations: Arsenic (V) adsorbed on gibbsite, *Geochim. Cosmochim. Acta* 65 (2001) 1211-1217.
- [55] J.R. Bargar, S.N. Towle, G.E. Brown, G.A. Parks, XAFS and bond-valence determination of the structures and compositions of surface functional groups and Pb(II) and Co(II) sorption products on single-crystal α -Al₂O₃, *J. Colloid and Interface Sci.* 185 (1997) 473-492.
- [56] C.C. Davis, H.-W. Chen, M. Edwards, Modeling silica sorption to iron hydroxide, *Environ. Sci. Technol.* 36 (2002) 582-587.
- [57] J. Crank, *The Mathematics of Diffusion*, 2nd ed., Oxford Science Publications, Oxford, UK, 1975.

[58] M.J. DeMarco, A.K. SenGupta, J.E. Greenleaf, Arsenic removal using a polymeric/inorganic hybrid sorbent, *Water Res.* 37 (2003) 164-176.

[59] S. Padungthon, J. Li, M. German, A.K. SenGupta, Hybrid anion exchanger with dispersed zirconium oxide nanoparticles: A durable and reusable fluoride-selective sorbent, *Environ. Eng. Sci.* 31 (2014) 360-372.

ACCEPTED MANUSCRIPT

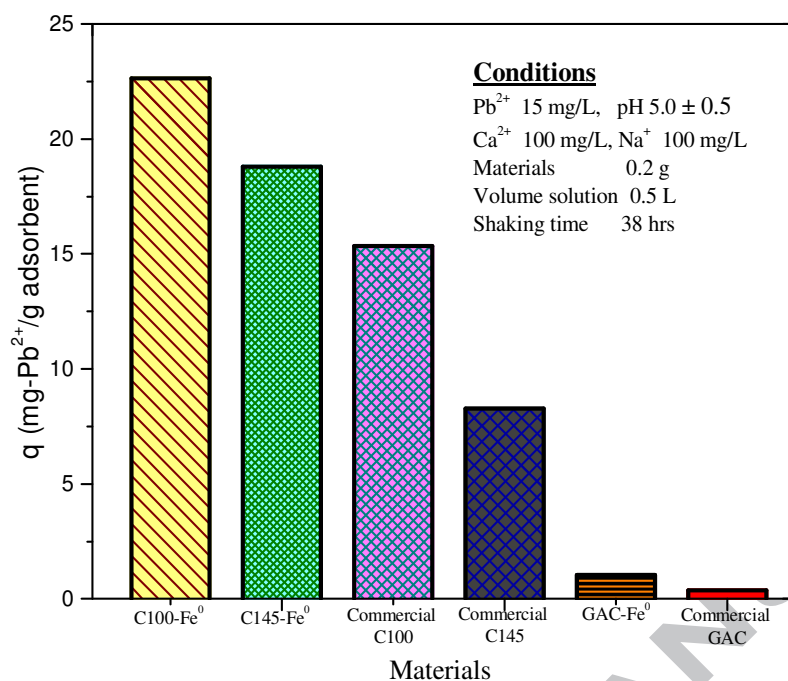


Fig 3 Batch equilibrium tests for lead removal using various adsorbents

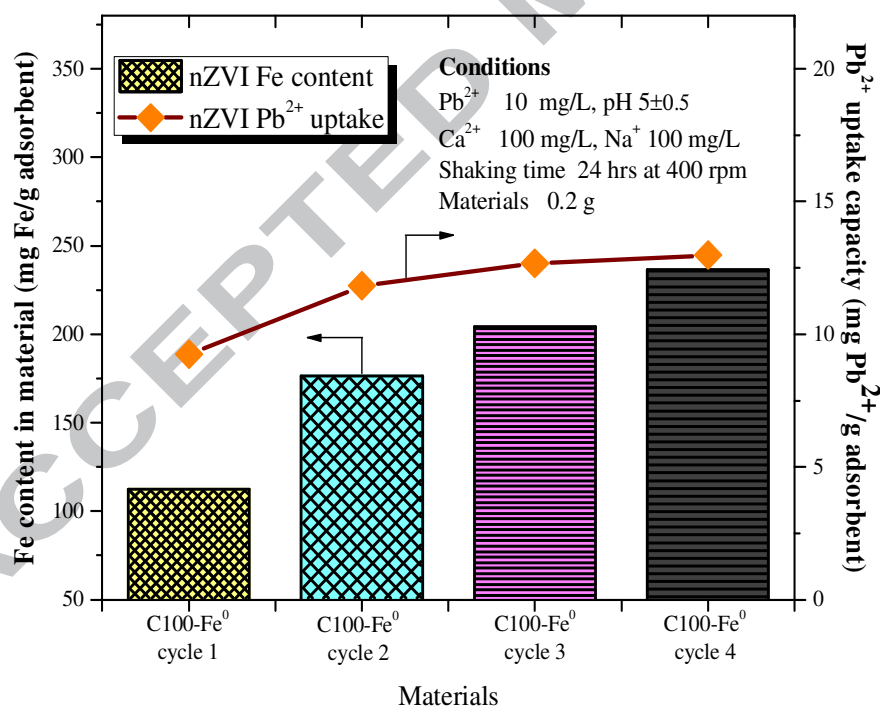


Fig. 4 Effect of nZVI loading cycles on the amount of iron dispersed within the hybrid cation exchanger and on the corresponding Pb^{2+} uptake capacity.

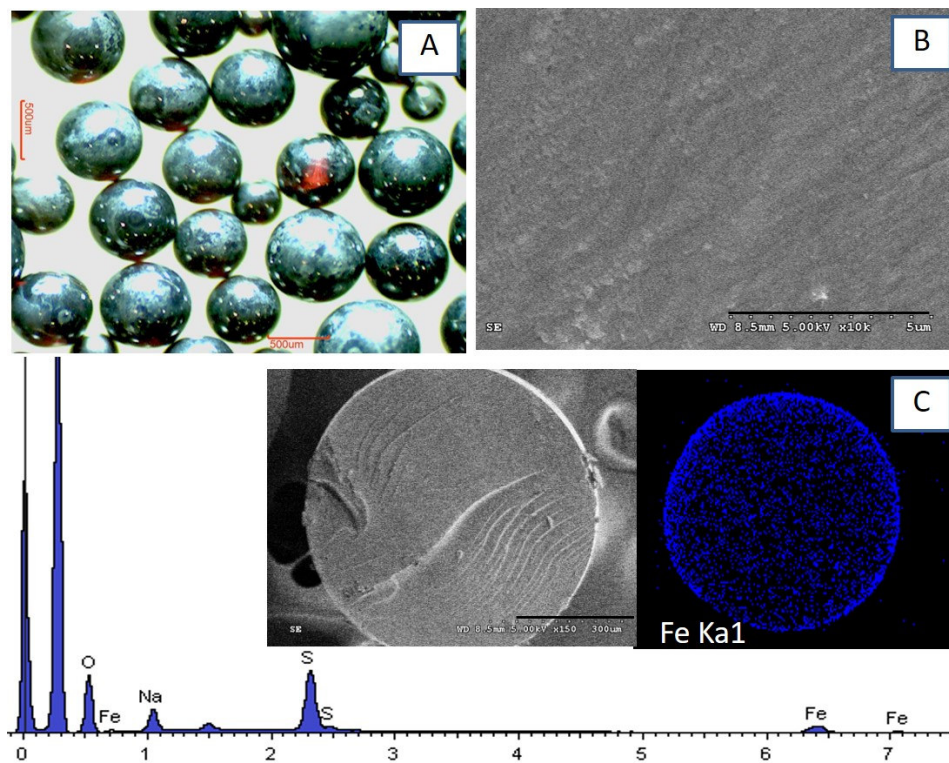


Fig. 5 (A) Enlarged view photograph of the C100-Fe⁰ (~500 μm diameter bead); (B) SEM of gel-type C100-Fe⁰ (10,000X); (C) Energy dispersive X-ray spectroscopy (EDX) spectrum of the material (10% Fe w/w) including iron mapping.

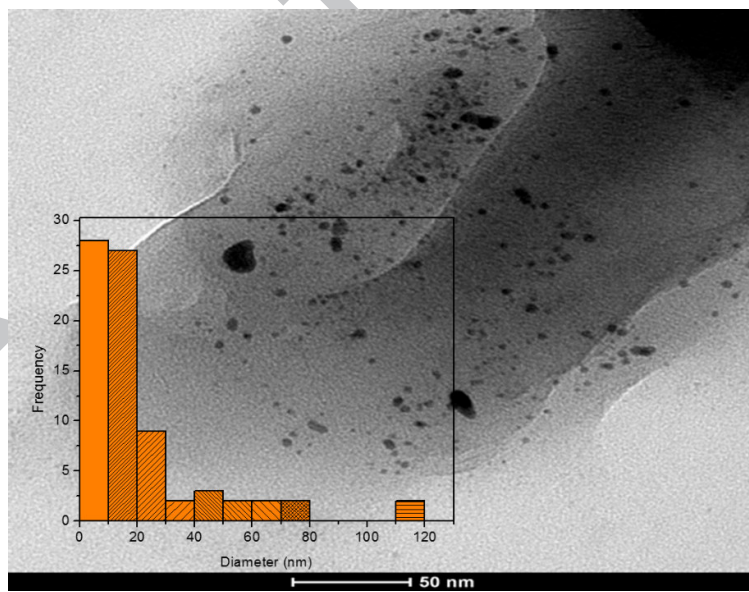


Fig. 6 Transmission electron microscopy (TEM) of C100-Fe⁰

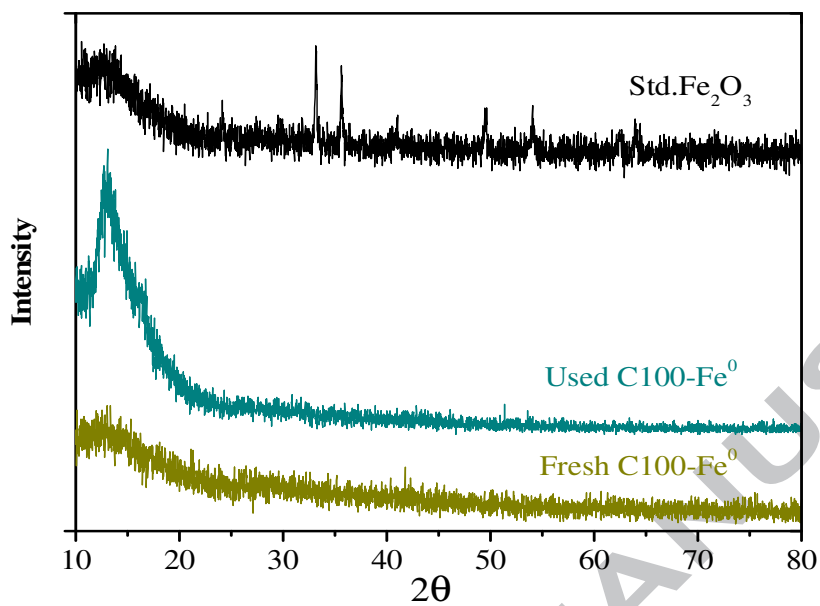


Fig. 7 Comparison of XRD diffractograms between a freshly prepared C100-Fe⁰ and used C100-Fe⁰ with standard Fe₂O₃.

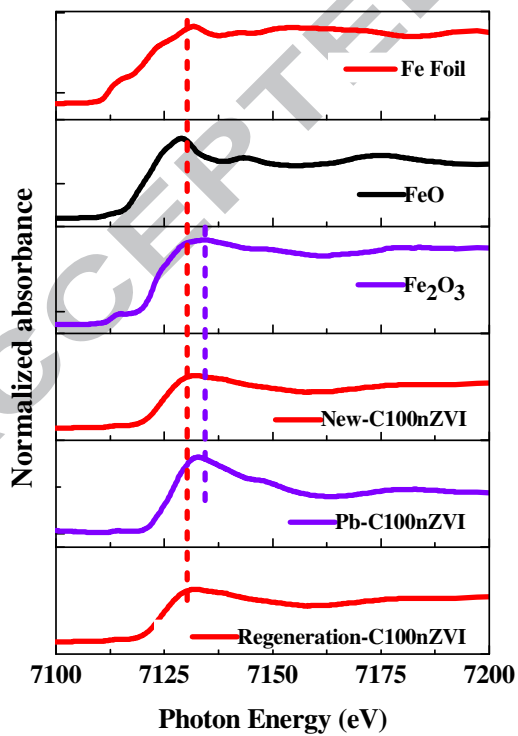


Fig. 8 XANES spectra for C100-Fe⁰ samples comparing with Fe⁰, Fe²⁺ and Fe³⁺ standards.

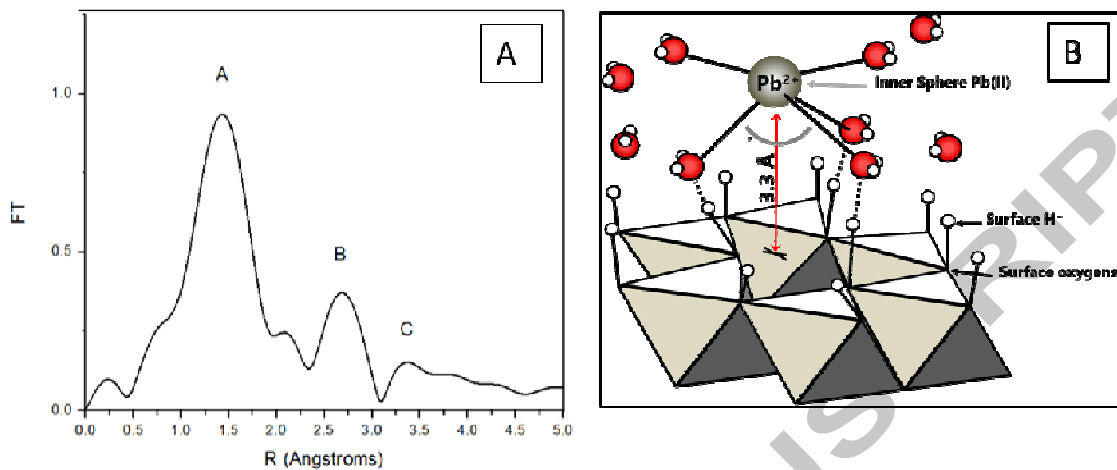


Fig. 9 (A) EXAFS results at Fe K-edge and (B) Proposed Pb adsorption onto the surface of iron oxide through the formation of bidentate inner-sphere complex.

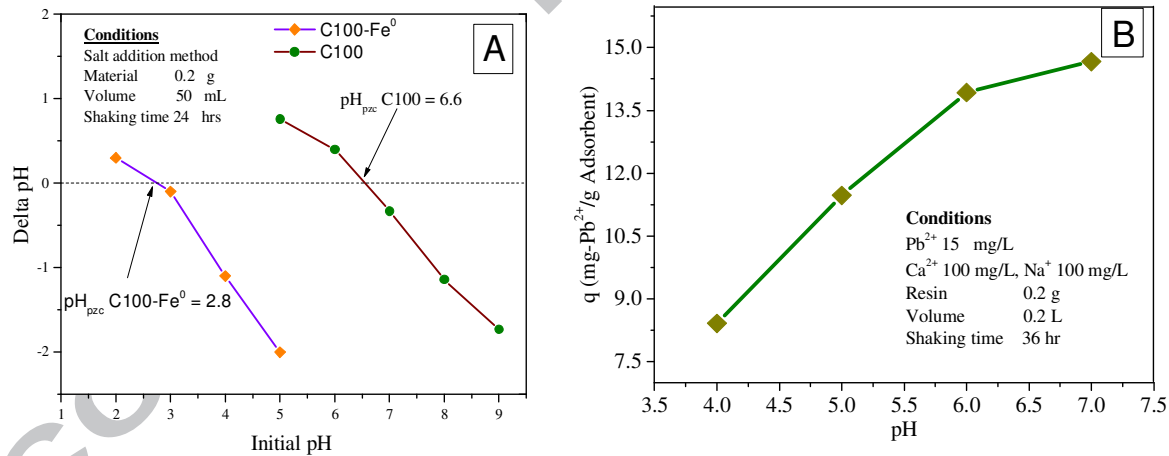


Fig. 10 (A) Δ pH versus initial pH of C100-Fe⁰ in 0.1 M NaCl solution at 298 K. (B) Effect of pH of C100-Fe⁰.

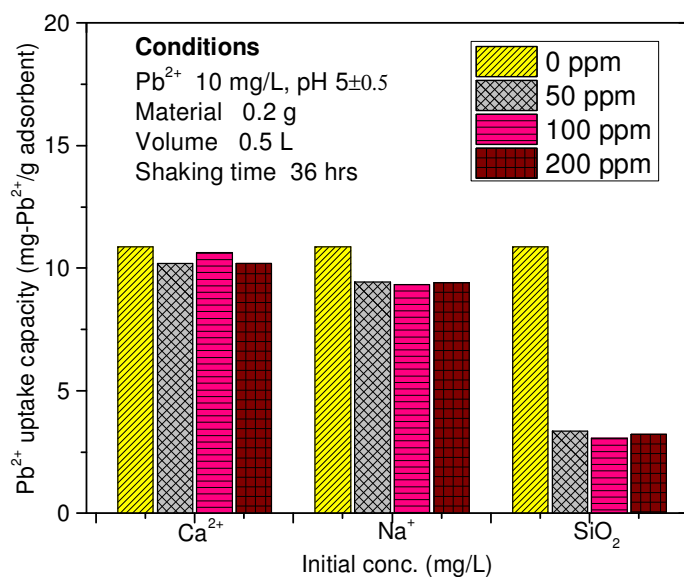


Fig. 11 Effect of competing ions on Pb(II) removal capacity.

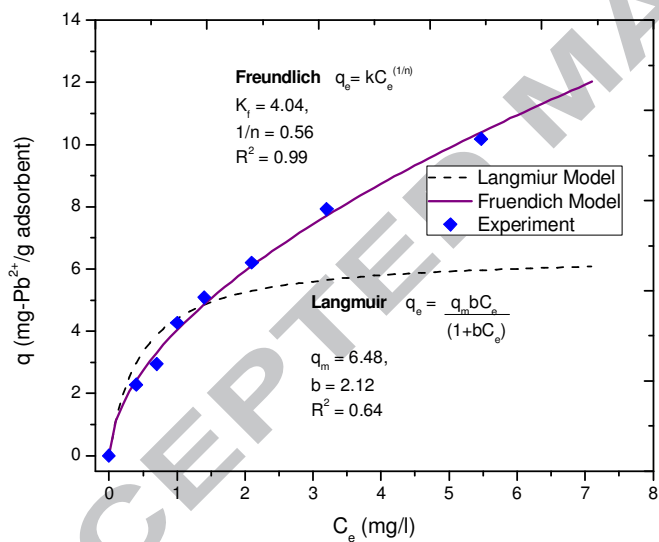


Fig. 12 The comparison of Pb(II) adsorption by C100-Fe⁰ between Langmuir and Freundlich Models (Non Linear).

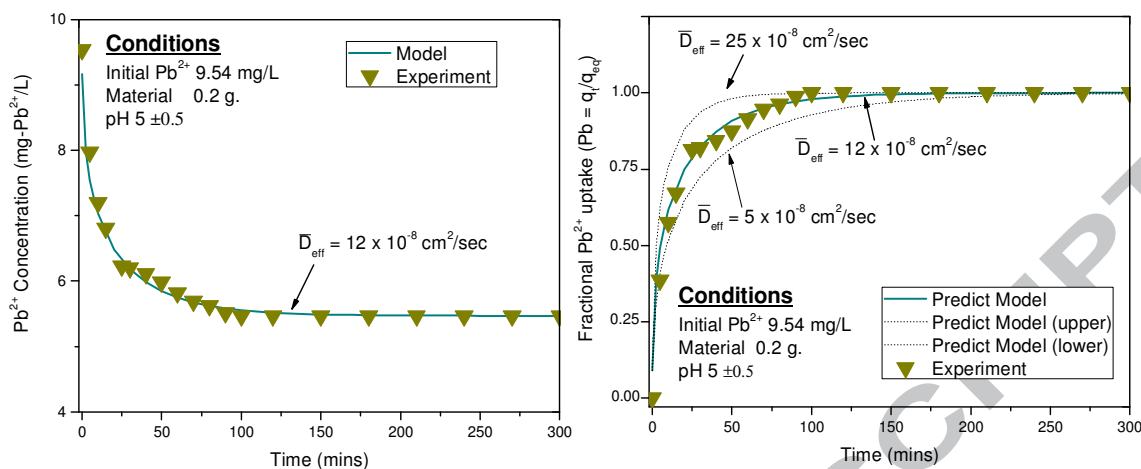


Fig. 13 (A) Aqueous lead concentration versus time during the batch kinetic test using C100-Fe⁰, (B) fractional lead uptake (q_t / q_{∞}) versus time (t) from the batch kinetic test result in (A).

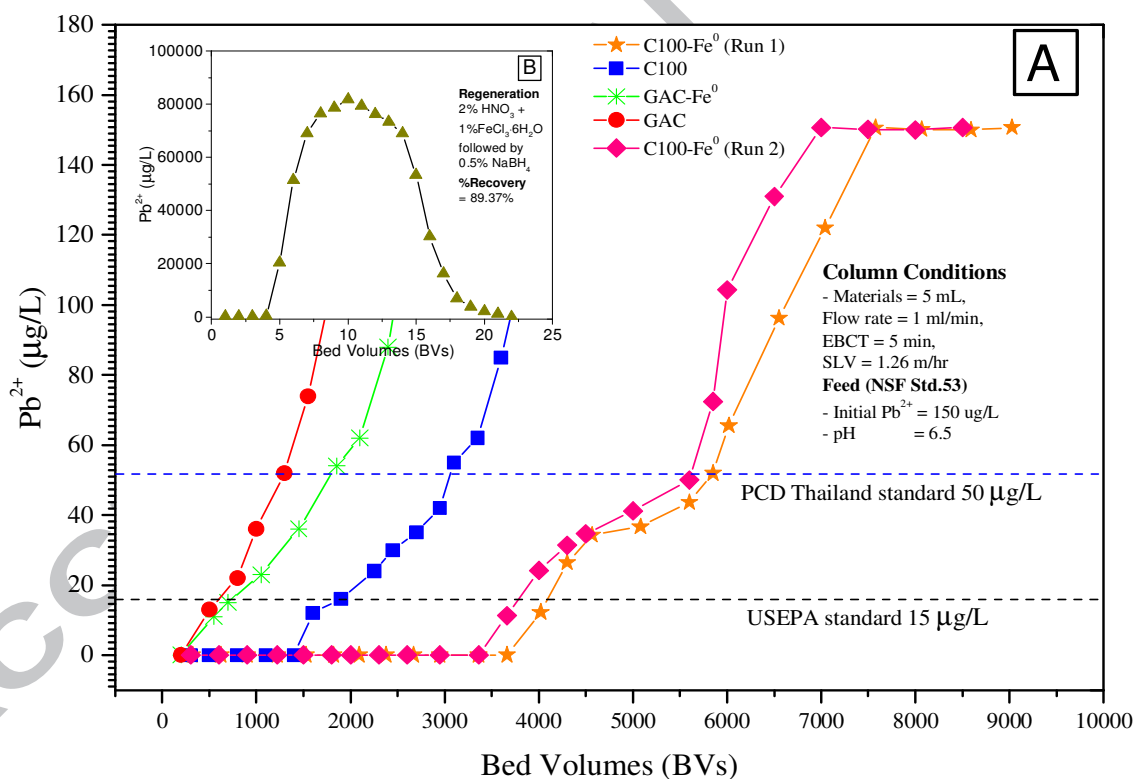


Fig. 14 (A) Pb(II) removal on fixed-bed column runs using four different materials, namely, hybrid cation (C100-Fe⁰), hybrid granular activated carbon support nZVI (GAC-Fe⁰), commercial cation exchange resin (C100), and commercial granular activated carbon (GAC) (B) Regeneration of C100-Fe⁰.

Highlights

- A new lead selective adsorbent (C100-Fe⁰) has been prepared with size range 20 nm.
- The material is reusable, durable and can be synthesized onsite.
- The inner-sphere surface complexes between lead and iron were observed by EXAFS.
- Lengthy fixed-bed column runs were used to validate the performance and reusability of C100-Fe⁰.

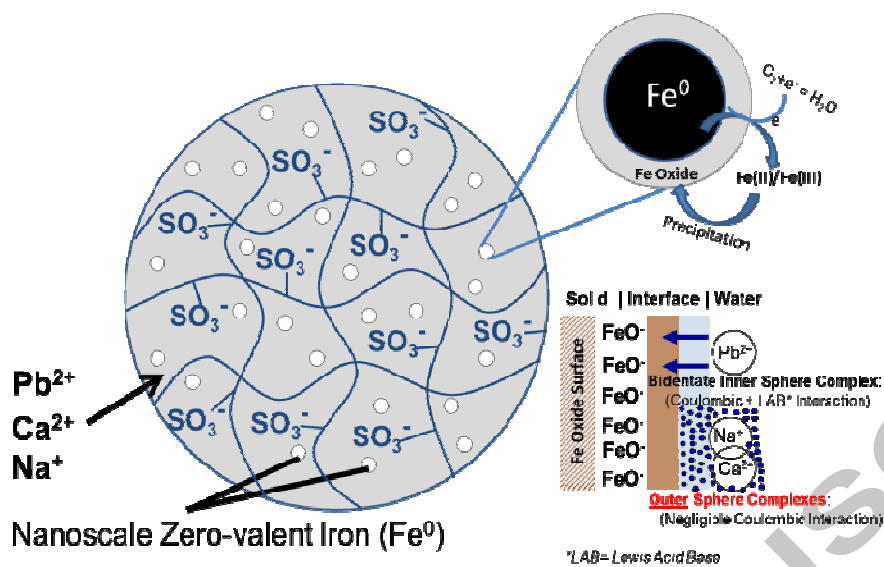


Fig. 1 Diagram of a reusable gel cation exchanger containing nano-scale zero valent iron (C100-Fe⁰).